



Semi-automated analysis of embryoscope images: using localized variance of image intensity to detect embryo developmental stages

Journal:	<i>Cytometry: Part A</i>
Manuscript ID:	14-081.R1
Wiley - Manuscript type:	Original Article
Date Submitted by the Author:	n/a
Complete List of Authors:	Mölder, Anna; Manchester Metropolitan University, Department of Sensory and Biological Computation Drury, Sarah; Division of Reproductive Health, Warwick Medical School; Centre for Reproductive Medicine, University Hospitals Coventry and Warwickshire NHS Trust Costen, Nicholas; School of Mathematics, Computing and Digital Technology, Manchester Metropolitan University Hartshorne, Geraldine; Division of Reproductive Health, Warwick Medical School; Centre for Reproductive Medicine, University Hospitals Coventry and Warwickshire NHS Trust Czanner, Silvester; School of Mathematics, Computing and Digital Technology, Manchester Metropolitan University
Key Words:	Automated image analysis, Image-based embryo classification, Computer-aided diagnosis, Automated annotation, Time-lapse microscopy, Embryoscope, Embryology

SCHOLARONE™
Manuscripts

1
2
3
4
5
6
7
8
9
10
11
12
13
14
15
16
17
18
19
20
21
22
23
24
25
26
27
28
29
30
31
32
33
34
35
36
37
38
39
40
41
42
43
44
45
46
47
48
49
50
51
52
53
54
55
56
57
58
59
60

EMBRYO DEV. STAGES USING LOCALIZED VARIANCE

1

1 **Credit**

2 Funding for the present study was provided by Manchester Metropolitan University, the Biomedical
3 Research Unit in Reproductive Health, University Hospitals Coventry and Warwickshire NHS Trust,
4 UK and Warwick Medical School.

5

For Peer Review

6 Introduction

7 In Vitro Fertilization (IVF) has been in clinical use for more than 30 years. Nevertheless, there is scope
8 for improvement of the embryo selection procedure. By refining selection based upon a greater
9 understanding of embryo quality, we could not only reduce multiple births, but also save patients the
10 cost and distress of multiple failed attempts. Time-lapse imaging of embryos offers the prospect of
11 such improvements and recent advances in incubator and imaging technology have enabled frequent
12 observation and image capture of individual embryos at intervals of a few minutes. However, with the
13 increased amount of generated imaging data it is essential to find quality markers suitable for
14 automated detection via computer-aided diagnostic tools. This technology has also opened up a new
15 area of research studying the impact of timing of key occurrences in embryo development. Currently,
16 key events require to be identified and annotated manually, which is time-consuming and limits the
17 usefulness of the instrumentation. Non-invasive markers suitable for computer-aided diagnosis are
18 being sought to standardize embryo selection procedures, speed up the annotation process and
19 provide diagnostic support.

20 Embryo quality is well known to relate to embryo morphology (1,2,3), but is not sufficiently precise an
21 indicator to predict outcome reliably in individual patients. Embryo evaluation today is commonly
22 undertaken using annotations of relevant features by experts at intermittent time points during
23 development. Attempts have been made to standardize manual selection (4) and decision support
24 systems exists for evaluating embryos (5,6,7,8,9). However, manual annotation is time-consuming and
25 the evaluation will vary according to the observer and the different clinical conventions used (10).
26 Automatic procedures to aid annotation would make the analysis less subjective and greatly reduce
27 the manual workload involved.

28 Many reports have highlighted the need to observe embryo development dynamically
29 (11,12,13,14,15). To thoroughly assess the benefits and drawbacks of time-lapse embryo imaging,
30 large scale randomized clinical studies need to be performed, but before they can be done, at least
31 two vital steps remain: The identification of the most promising markers to use and the set-up of a
32 system capable of collecting and analyzing large amounts of embryo data in a standardized and

EMBRYO DEV. STAGES USING LOCALIZED VARIANCE

3

33 robust manner and consistency in evaluation is crucial to the usefulness of results. When migrating
34 from a manual to an automated system, it may not be possible to require 1:1 correspondence between
35 measurements, if the two selections are made based on distinctly different criteria. In these cases, a
36 comparison must be made between manual and automatic evaluation, in order to establish the
37 presence and size of any offset. Such comparative studies will need not only expertise in current
38 methodology in both current embryo selection procedures and manual annotation, but also a firm
39 understanding of computerized image analysis and the nature of the image material used.

40 Several systems for automated embryo analysis using various approaches have previously been
41 reported. One time-lapse system available uses an image-based decision tool analyzing cleavages to
42 the four cell stage using dark field optics (16). A few systems rely on direct modeling of physical
43 conditions (17,18), requiring a highly controlled environment as well as detailed knowledge of the
44 optical setup, something which is not always possible under clinical conditions. Other systems perform
45 pattern recognition on microscopic images. Usually, a correctly performed segmentation (18,19,20,21)
46 provides the most detailed information on blastomere position, shape and outline, but this can be
47 prone to errors, especially when used under clinical circumstances where complete and accurate
48 segmentation may not always be possible. Using a semi-automatic approach, where a region of
49 interest has been selected manually (22,23,24), it is often possible to perform various computer vision
50 and pattern recognition tasks even in a clinical setting. However, with a manual input required to
51 initialize computation, this approach may instead increase user interaction with images, making it more
52 suitable for in-depth research purposes than for routine clinical work or large scale studies.

53 As an alternative, this study investigates the possibility of accessing relevant information using
54 variations in image grey level in bright field images. The result is a framework for the detection of key
55 events in embryo development without requiring sample-wise initialization. At the same time, a
56 graphical interpretation of embryo development as viewed *in vitro* is presented, serving as a
57 complement to manual inspection of images.

58 **Materials and Methods**

59 **Embryo culture and image capture**

60 Time lapse image series of human embryos fertilized *in vitro* were acquired as anonymized sequences
61 of human embryos donated to research with ethical approval from Coventry Research Ethics
62 Committee (04/Q2802/26) and the Human Fertilisation and Embryology Authority (R0155). Embryos
63 were cultured in 25µl culture media (Origio, Redhill, UK) under mineral oil for up to 6 days, incubated
64 at 37°C in an atmosphere of 5%CO₂, 5%O₂, 90%N₂. The images were captured using the
65 Embryoscope® system (Unisense Fertilittech, Copenhagen, Denmark), with up to 7 focal depth planes,
66 15-25 µm apart, recorded at 20 minute intervals using a Hoffman Modulation Contrast (HMC) optical
67 set up (25) and a 635nm LED as light source. Fresh medium was supplied at intervals, but embryos
68 were otherwise undisturbed during imaging. The total dataset consisted of image series of 39 embryos
69 from seven different couples, of which 28 developed into blastocysts. Fourteen series of embryos (of
70 which nine developed blastocysts) were used in an initial study (referred to as training set) to optimize
71 algorithm parameters, and the analysis was repeated using the same parameters for the remaining 25
72 embryos (of which 18 developed blastocysts). The latter is referred to as the test set.

73 **Software implementation**

74 Series of stacks of HMC images with a grey scale ranging from 0-255 provided the raw material for
75 this study. In HMC microscopy, changes in optical path length are optically converted to light and dark
76 gradients on an even grey background, resulting in an image where edges are the most prominent
77 structures. As the number of edges in the image increases, the two dimensional distribution of image
78 intensity changes. Objects in embryo development expected to result in an increased number of edges
79 are visible nuclei and pronuclei as well as an increased number of blastomeres. Conversely,
80 compaction and loss of focus are expected to increase image smoothness, following a loss of edge
81 structures. Image variance is a measure of the distribution of grey levels within a specified region of
82 the image and will increase with an increased number of edge structures. It is the hypothesis of this

EMBRYO DEV. STAGES USING LOCALIZED VARIANCE

5

83 study that variance as a measure of edge structures can be used as an indirect method to identify the
84 timing of embryo developmental stages.

85 In order to detect fluctuations in variance with sufficient sensitivity to distinguish changes caused by,
86 for example the appearance of a nucleus, two pre-filtering steps were necessary. The first step, which
87 was used for every image series, selected one focal level in the stack as containing the optimal focus.
88 This resulted in a sequence of single captures (Figure 1a). The process is described further in the
89 supplementary material (Appendix A). The second step, performed on each remaining capture,
90 automatically detected the outline of the embryo using a circular Hough Transform. From the outline,
91 the internal region of the embryo was selected as a circular region of interest (ROI) at half the embryo
92 radius, as described in (26). The localized variance in image intensity was then calculated for the
93 selected ROI of each image. Figure 2 shows an example of the breakdown of pronuclei, and its effect
94 on image variance. For the duration of the cleavage stage, it was assumed that no entire blastomere
95 would appear completely outside the ROI. For the blastocyst stage, the choice of region proved useful
96 since the formation of the trophectoderm removed in-focus blastomeres from the embryo interior to the
97 outline of the blastocyst (outside the ROI) making the finished blastocyst appear with a characteristic
98 drop in image variance, once the cavity was formed. Figure 1b shows an example of an embryo
99 growing *in vitro*, as viewed with the image intensity variance of the embryo interior.

100 Next, images were examined visually for key occurrences in embryo development, and the same
101 events were evaluated using the image variance, constructing two characteristic profiles of a growing
102 embryo, one obtained by manual observation and one by mathematical inspection. The accuracy of
103 the hypothesis is defined by the correlation between the two profiles. The following details were
104 included in the profile: The timing of the pronuclear breakdown preceding syngamy (PNB), the timing
105 of the first mitotic divisions up to 8 cell stage and the transitions between a chosen set of main
106 developmental stages. The details of the profiling are explained further in supplementary material
107 (Appendix B-D). A brief summary is given below.

108

109 Detection of Syngamy

110 For automatic detection of the PNB, a single threshold was optimized using the 14 training embryos.
111 The timing of the PNB was computed for a number of thresholds, and the minimum value giving 10%
112 true positive detection (when comparing to visual inspection of the images of the training embryos)
113 was selected and used for the testing embryos.

114 Cleavage divisions

115 Mitotic divisions were also detected using a single threshold.

116 Compaction and blastocyst formation

117 Five stages were selected as being of interest: Cleavage (A), Compaction (B), Morula (C), Cavitation
118 (D) and Blastocyst (E (Figure 1b). The timing of transition between stages was defined as:

119 AB: Main local maxima in variance, located before the main negative gradient.

120 BC: Main negative gradient in variance.

121 CD: Main positive gradient in variance, located after the main negative gradient.

122 DE: Main local maxima in variance, located after the main negative gradient.

123 The computationally obtained stages and the transitions between stages were given letters in order to
124 distinguish them from the visually defined embryo stages. For instance, the stage 'B' is defined
125 mathematically as the main negative gradient in variance, and it is part of the hypothesis that this
126 relates to the formation of the compaction stage of the embryo. Finally, six traits for the developmental
127 stages were combined and used simply to detect the presence or absence of a blastocoel. The six
128 characteristics used were:

129 – The width (duration) of the negative gradient at compaction (B).

130 – The height of the maximum variance detected at the end of the cleavage stage (AB).

131 – The height of the maximum variance detected at cavitation (DE).

132 – The timing of compaction (B).

EMBRYO DEV. STAGES USING LOCALIZED VARIANCE

7

- 1
2
3
4
5
6 133 – The timing of the maximum at the end of the cleavage stage (AB).
7
8 134 – The total number of variance gradients during the entire development (a sign of strong
9
10 135 fluctuating behavior, indicating poor quality).
11

12
13 136 The six traits were combined into four parameter sets, and the threshold for each one varied, while
14
15 137 measuring the number of detected blastocyst formations.
16

138 **Expert validation and statistical analysis**

139 Last, a total of 15 time-lapse image series from four different patients were used for validation. The
140 timing of cell divisions and embryo stages was validated against the opinion of five expert clinical
141 embryologists, each with at least 6 years of clinical embryology experience. The rest of the image
142 series were annotated by the experimenters to the best ability using the same criteria as the
143 embryologists. One image series was evaluated by all five experts, to allow direct comparison of their
144 assessments. The annotation of timing in images was consistently within 1-3 time frames up to an 8-
145 cell stage, and the overall quality of the embryo in 100% agreement (Figure 3). P-values equal or
146 inferior to 0.05 was used for statistical significance. Intervals in graphs and for values are given as
147 means \pm SD unless otherwise stated.
18
19
20
21
22
23
24
25
26
27
28
29
30
31
32
33
34
35
36
37
38
39
40
41
42
43
44
45
46
47
48
49
50
51
52
53
54
55
56
57
58
59
60

148 **Results**

149 For embryos where developmental stages were visible in images, they were also reflected in the
150 variance profile (Figure 4). Both by manual observation and as measured by variance, large
151 differences were apparent between individual embryos.

152 **Detection of syngamy**

153 In Figure 4b, the PNB is visible in the plot of variance vs. image capture time as a sudden negative
154 gradient over the course of 1-2 frames. Twenty images per embryo for the training set of 14 embryos
155 were selected before and after PNB and used to profile the change of state. The difference in variance
156 before and after the breakdown was large enough to be detectable, despite individual variation
157 between images (Figure 2c). The breakdown usually took less than one or two captures, giving an
158 uncertainty of the timing of detection of at most 40 minutes at the current capture frequency. Requiring
159 a 100% true positive detection of the PNB for all 14 training embryos, the best overall result was 88%
160 accuracy for the training embryos, the inaccuracy being caused by false positive detection. Using the
161 same settings for the 25 test embryos, an overall detection accuracy of 90% was achieved, with 91%
162 true positive detection (Figure 2d).

163 **Cleavage divisions**

164 In total, 37 of 39 image series had sufficient quality to detect the first five mitotic divisions. Two
165 embryos were excluded because of heavy optical interference. For most time series, it was possible to
166 use the first automatically detected cell divisions, but manual adjustments were made in a few cases
167 where both the division between 2-3 cells and between 3-4 cells appeared within the 20 minute gap
168 between captures. Computational detection was compared to manual detection for divisions of up to
169 the 4 cell and 8 cell stages, as shown in Figure 5. For embryos at the 1-8 cell stage, there was a clear
170 bias towards divisions being under-detected when using the automated procedure. For embryos at 1-4
171 cells, no more than two false positives (detection of divisions that were not present) or false negatives
172 (failure to detect divisions) occurred per time series. From Figure 3c, it is apparent that the uncertainty
173 in the exact location of division increases with the number of blastomeres. From the total image set of

EMBRYO DEV. STAGES USING LOCALIZED VARIANCE

9

174 37 embryos, 100% of divisions from 1 to 2 cells were detected, 73% from 2 to 3 (or 4) cells, 30% from
175 3 to 4 cells, and 59% from 4 to 5 (or 6) cells. The three and five cell stages were not always
176 distinguishable using a image capture frequency of 20 min. Of all divisions between 1-6 cells, 62% of
177 divisions were located at the same captured frame index using both computer and manual detection,
178 and 76% of divisions were located within one captured frame index from the manually noted position.
179 The same values for the manual detection, as compared to the mean of the expert annotation, were
180 35% exact location, and 74% within one time frame. For the 28 embryos which eventually formed a
181 blastocyst, a measurement was also made of the time elapsed between the automatically detected cell
182 divisions from 2 to 3 cells and from 3 to 4 cells on the total set of 39 image series, resulting in 10.27+/-
183 2.66 h (2-3 cells), and 1.11+/-1.34 h (3-4 cells), respectively.

184 Compaction and blastocyst formation

185 Manual annotation by experts showed less agreement on timing of transitions between developmental
186 stages (Figure 4b), compared to detection of division. For automatic detection, the mean and gradient
187 of the variance for each of the stages A-E was computed for each embryo. The results are shown in
188 Figure 5. The change in variance per unit time during the compaction and the cavitation stage was
189 one order of magnitude higher than that for the entire cleavage stage, typically 0.3 h^{-1} . All values
190 showed a high degree of variation (commonly with standard deviations in the range of 60-80%)
191 between embryos. Interestingly, there was a distinct difference between embryos from different
192 patients, when the duration of the four stages A-D was measured (Figure 6). The duration of the
193 morula stage showed high variability among embryos from the same patient, whereas the duration of
194 the cleavage stage and the cavitation stage had a higher inter-patient than intra-patient variability. The
195 compaction stage, morula stage and cavitation stage had approximately the same duration, about 1/7
196 that of the cleavage stage. However, the duration of the cleavage stage was only approximately
197 determined since the exact time of fertilization was unknown for the series analyzed. Finally, the
198 detected transitions and relative height of variance local maxima and gradients were combined and
199 used to classify each embryo in two groups; those forming blastocysts, and those failing to do so. The
200 results were evaluated by visual inspection of the captured image series. The best overall result was

EMBRYO DEV. STAGES USING LOCALIZED VARIANCE

10

- 1
2
3
4
5
6
7
8
9
10
11
12
13
14
15
16
17
18
19
20
21
22
23
24
25
26
27
28
29
30
31
32
33
34
35
36
37
38
39
40
41
42
43
44
45
46
47
48
49
50
51
52
53
54
55
56
57
58
59
60
- 201 correct detection of a blastocyst being formed in 71.8% of cases, but at a cost of 28.2% false positive
202 detection (computational indication of a blastocyst without actual blastocyst formation), with little
203 sensitivity to parameter setting (Figure 7).

For Peer Review

204 Discussion

205 The method of locating the timing of mitotic divisions shows a larger span between maximum and
206 minimum deviation from the true position compared to manual detection, but on average, our method
207 performed better. 62% of cleavages identified by automatic detection were located at the exact same
208 capture frame as manually identified by experts. The same agreement for manual detection between
209 different experts was only 35%, showing the potential of automated image analysis to increase
210 objectivity and consistency of embryo analysis. If instead we define a correct detection to be within
211 one captured frame of the control (corresponding to a timing inaccuracy of 20 min), the manual and
212 computed accuracy were both approximately 75%. The results of the automatic method improved if
213 only the 1-4 cell stages were considered, compared to all 1-8 cell stages. The results depend heavily
214 upon the frequency of image capture - 20 minutes for this study - which was long enough for most cell
215 divisions to take place over the course of several captured frames, but we experienced difficulty in
216 distinguishing the three, five and seven blastomere stages at this capture frequency. With more
217 images captured and analyzed per unit time, it is possible that the uncertainty in location in terms of
218 image index may increase, while at the same time decrease if computed for clock time. In measuring
219 the timing of the first few mitotic divisions, the results overlap, but have higher standard deviations
220 than a previously reported study (27). However, the results for (27) were obtained with visual counting
221 of mitotic divisions, whereas the timing of divisions in the present study were automatically computed.

222 In detecting embryonic developmental stages, there were large variations between individual embryos,
223 as expected from clinical experience. In spite of this, a clear trend in the variance profile was apparent,
224 and we have shown that it was possible to identify the formation of a blastocyst by automated image
225 analysis in >70% of cases. It was also apparent that the definition of stages and transitions using the
226 localized variance was different from that of manual detection, indicating that this way of visualizing
227 blastocyst development may serve best as a complement to inspection of images by eye.

228 The parameters for the detection of blastocyst formation depend on the frequency of image capture
229 and the hardware settings, adding a requirement for a calibration stage before analysis. For future

EMBRYO DEV. STAGES USING LOCALIZED VARIANCE

12

230 work, a comparison between different image capture frequencies would be desirable. It is also evident
231 that the exact appearance of the variance function $v(t)$ depended on the choice of the region of
232 interest. In this study, selecting a circular region of four different radii were investigated. Also,
233 parameters for this study (Appendix D) were chosen as the most feasible using our current knowledge
234 of embryo development. The implication of any choice of parameters should be further evaluated
235 before taking on a larger scale study, since it is possible that new technical tools to study embryos will
236 also require new methods to define embryos health. Furthermore, there is a trade-off between
237 minimizing false negative and false positive detection. For our purpose of automating annotation, it
238 was decided that false negatives were undesirable, whereas false positives could be acceptable and
239 handled in a future manual or automatic filtering step. This decision may change depending on the
240 intended purpose of detection. Also, to improve the accuracy this framework could be expanded using
241 more extractable image cues. For example local image texture or measurements based on direct
242 recognition of blastomere outlines could be used. Last, the use of an automatic image analysis is
243 dependent on initial image quality, and for larger studies it will be necessary to establish robustness
244 under clinical conditions.

245 There are reasons for caution in evaluating embryo quality since all studies of embryos before
246 implantation will per definition only be able to assess embryo quality, not taking into account the
247 uterine component of implantation. In IVF treatment, one or more embryos are normally selected for
248 transfer to the uterus on days 2, 3 or 5-6 of development, when those developing in a normal and timely
249 manner are usually at the 4-cell, 8-cell or blastocyst stages respectively. However, many embryos harbour
250 abnormalities that render them incapable of prolonged development and some of these abnormalities
251 become manifest during pre-implantation development as abnormal, delayed or arrested growth. Thus,
252 embryos transferred at the blastocyst stage are more likely to result in pregnancy than those transferred at
253 earlier stages. Blastocyst transfer is therefore associated with a higher chance of pregnancy and is the
254 latest stage at which pre-implantation selection can be carried out. Recent results (15) show that time-
255 lapse studies of earlier embryonic stages can predict blastocyst development, but that the formation of
256 a blastocyst is not necessarily an indication of a live birth outcome. In this study, we defined blastocyst
257 formation to be evidence of a good quality embryo, but for future work we shall extend this study to

EMBRYO DEV. STAGES USING LOCALIZED VARIANCE

13

258 clinical data where success in terms of initiating pregnancy and resulting in a live birth is known. Still,
259 there is a need for prediction of blastocyst formation (28) and the ability for negative prediction, i.e. de-
260 selection of unsuitable embryos, has the potential to save resources and allow for a more robust
261 selection of single successful embryos for transfer. This could be achieved using automated analysis
262 of previously identified parameters, such as immediate cleavage.

263 In conclusion, it is shown here that key events in pre-implantation embryo development can be
264 detected using a simple automated approach to embryo time-lapse image analysis, offering the
265 potential of semi-automated annotation of clinical images on a large scale. The skills of the
266 embryologist may then be better focused on checking and correcting a reduced number of uncertain
267 computations, rather than performing routine manual annotation of the complete image set.

1
2
3
4 EMBRYO DEV. STAGES USING LOCALIZED VARIANCE

14

5
6
7
8 268 **Acknowledgements**9
10 269 None of the data here would be of any use, if not checked and evaluated by Ben Lavender, Pavan
11 270 Kachhwaha and Dr. Deborah Taylor of the Centre for Reproductive Medicine, University Hospitals
12 271 Coventry and Warwickshire NHS Trust. In addition, Unisense Fertiliteltech helped greatly by providing
13 272 images to complete the study. Finally, we would also like to thank Dr. Gabriela Czanner for invaluable
14 273 help in evaluating the statistics.
15
16
17
18
19
20
21
22
23
24
25
26
27
28
29
30
31
32
33
34
35
36
37
38
39
40
41
42
43
44
45
46
47
48
49
50
51
52
53
54
55
56
57
58
59
60

274 **References**

- 275 1. Schoolcraft WB, Gardner DK, Lane M, Schlenker T, Hamilton F, Meldrum DR. Blastocyst culture
276 and transfer: analysis of results and parameters affecting outcome in two in vitro fertilization programs.
277 *Fertil Steril* 1999;**72**:604–609.
- 278 2. Sakkas D, Percival G, D'Arcy Y, Sharif K, Afnan M. Assessment of early cleaving in vitro fertilized
279 human embryos at the 2-cell stage before transfer improves embryo selection. *Fertil Steril*
280 2001;**76**:1150–1156.
- 281 3. Guerif F, Gouge A Le, Giraudeau B, Poindron J, Bidault R, Gasnier O, Royere D. Limited value of
282 morphological assessment at days 1 and 2 to predict blastocyst development potential: a prospective
283 study based on 4042 embryos. *Hum Reprod* 2007;**22**:1973–1981.
- 284 4. Racowsky C, Vernon M, Mayer J, Ball GD, Behr B, Pomeroy KO, Winingar D, Gibbons W,
285 Conaghan J, Stern JE. Standardization of grading embryo morphology. *J Assist Reprod Genet*
286 2010;**27**:437–439.
- 287 5. Jurisica I, Mylopoulos J, Glasgow J, Shapiro H, Casper RF. Case-based reasoning in IVF:
288 prediction and knowledge mining. *Artif Intell Med* 1998;**12**:1–24.
- 289 6. Manna C, Patrizi G, Rahman A, Sallam H. Experimental results on the recognition of embryos in
290 human assisted reproduction. *Reprod Biomed Online* 2004;**8**:460–469.
- 291 7. Patrizi G, Manna C, Moscatelli C, Nieddu L. Pattern recognition methods in human-assisted
292 reproduction. *Int Trans Opin Res* 2004:365–379.
- 293 8. Kawamoto K, Houlihan CA, Balas EA, Lobach DF. Improving clinical practice using clinical decision
294 support systems: a systematic review of trials to identify features critical to success. *BMJ*
295 2005;**330**:765.

- 1
2
3
4 EMBRYO DEV. STAGES USING LOCALIZED VARIANCE 16
5
6 296 9. Morales DA, Bengoetxea E, Larrañaga P, García M, Franco Y, Fresnada M, Merino M. Bayesian
7
8 297 Classification for the Selection of In-Vitro Human Embryos Using Morphological and Clinical Data.
9
10 298 *Comput Methods Programs Biomed* 2008;104–116.
11
12
13 299 10. Sundvall L, Ingerslev HJ, Knudsen UB, Kirkegaard K. Inter- and intra-observer variability of time-
14
15 300 lapse annotations. *Hum Reprod* 2013;3215-3221.
16
17
18 301 11. Azzarello A, Hoest T, Mikkelsen AL. The impact of pronuclei morphology and dynamicity on live
19
20 302 birth outcome after time-lapse culture. *Hum Reprod* 2012;27:2649–2657.
21
22
23 303 12. Basile N, Meseguer M. Time-lapse technology: evaluation of embryo quality and new markers for
24
25 304 embryo selection. *Expert Rev Obstet Gynecol* 2012;7:175–190.
26
27
28 305 13. Cruz M, Garrido N, Herrero J, Pérez-Cano I, Muñoz M, Meseguer M. Timing of cell division in
29
30 306 human cleavage-stage embryos is linked with blastocyst formation and quality. *Reprod Biomed Online*
31
32 307 2012;25:371–381.
33
34
35 308 14. Kirkegaard K, Agerholm IE, Ingerslev HJ. Time-lapse monitoring as a tool for clinical embryo
36
37 309 assessment. *Hum Reprod* 2012;27:1277–1285.
38
39
40 310 15. Kirkegaard K, Kesmodel US, Hindkjær JJ, Ingerslev HJ. Time-lapse parameters as predictors of
41
42 311 blastocyst development and pregnancy outcome in embryos from good prognosis patients: a
43
44 312 prospective cohort study. *Hum Reprod* 2013;28:2643–2651.
45
46
47 313 16. Wong CC, Loewke KE, Bossert NL, Behr B, Jonge CJ De, Baer TM, Pera RAR. Non-invasive
48
49 314 imaging of human embryos before embryonic genome activation predicts development to the
50
51 315 blastocyst stage. *Nat Biotechnol* 2010;28:1115–1121.
52
53
54 316 17. Olsen NH. *Morphology and Optics of Human Embryos from Light Microscopy*. 2004; IT University
55
56 317 of Copenhagen, Department of Innovation.
57
58
59
60

- 1
2
3
4 EMBRYO DEV. STAGES USING LOCALIZED VARIANCE 17
5
6 318 18. Giusti A, Corani G, Gambardella LM, Magli MC, Gianaroli L. Blastomere segmentation and 3D
7
8 319 morphology measurements of early embryos from Hoffman Modulation Contrast image stacks. *2010*
9
10 320 *IEEE Int Symp Biomed Imaging Nano Macro* 2010;1261–1264.
11
12
13 321 19. Agerholm IE, Hnida C, Cruger DG, Berg C, Bruun-Petersen G, Kølvrå S, Ziebe S. Nuclei size in
14
15 322 relation to nuclear status and aneuploidy rate for 13 chromosomes in donated four cells embryos. *J*
16
17 323 *Assist Reprod Genet* 2008;**25**:95–102.
18
19
20 324 20. Morales DA, Bengoetxea E. Automatic segmentation of zona pellucida in human embryo images
21
22 325 applying an active contour model. *Proceedings of the 12th Annual Conference on Medical Image*
23
24 326 *Understanding and Analysis* 2008:209–213.
25
26
27 327 21. Filho ES, Noble JA, Poli M, Griffiths T, Emerson G, Wells D. A method for semi-automatic grading
28
29 328 of human blastocyst microscope images. *Hum Reprod* 2012;**27**:2641–2648.
30
31
32 329 22. Pedersen UD, Olsen, OF, Olsen, NH. A multiphase variational level set approach for modelling
33
34 330 human embryos. *Proceedings of the 2nd IEEE Workshop on variational, Geometric and Level Set*
35
36 331 *Methods*, 2003.
37
38
39 332 23. Hnida C, Engenheiro E, Ziebe S. Computer-controlled, multilevel, morphometric analysis of
40
41 333 blastomere size as biomarker of fragmentation and multinuclearity in human embryos. *Hum Reprod*
42
43 334 2004;**19**:288–293.
44
45
46 335 24. Beuchat A, Thévenaz P, Unser M, Ebner T, Senn A, Urner F, Germond M, Sorzano COS.
47
48 336 Quantitative morphometrical characterization of human pronuclear zygotes. *Hum Reprod*
49
50 337 2008;**23**:1983–1992.
51
52
53 338 25. Hoffman R. The modulation contrast microscope: principles and performance. *J Microsc*
54
55 339 1977;**110**:205–222.
56
57
58 340 26. Mölder A, Czanner S, Costen N, Hartshorne G. Automatic detection of embryo location using
59
60 341 rotational variance of the Hough Transform. *2014 22nd Int Conf Pattern Recognit ICPR* 2014;

EMBRYO DEV. STAGES USING LOCALIZED VARIANCE

18

- 1
2
3
4
5
6 342 27. Chavez SL, Loewke KE, Han J, Moussavi F, Colls P, Munne S, Behr B, Reijo Pera RA. Dynamic
7
8 343 blastomere behaviour reflects human embryo ploidy by the four-cell stage. *Nat Commun* 2012;**3**:1251.
9
10
11 344 28. Diamond MP, Willman S, Chenette P, Cedars MI. The clinical need for a method of identification of
12
13 345 embryos destined to become a blastocyst in assisted reproductive technology cycles. *J Assist Reprod*
14
15 346 *Genet* 2012;**29**:391-396.
16
17
18
19
20
21
22
23
24
25
26
27
28
29
30
31
32
33
34
35
36
37
38
39
40
41
42
43
44
45
46
47
48
49
50
51
52
53
54
55
56
57
58
59
60

For Peer Review

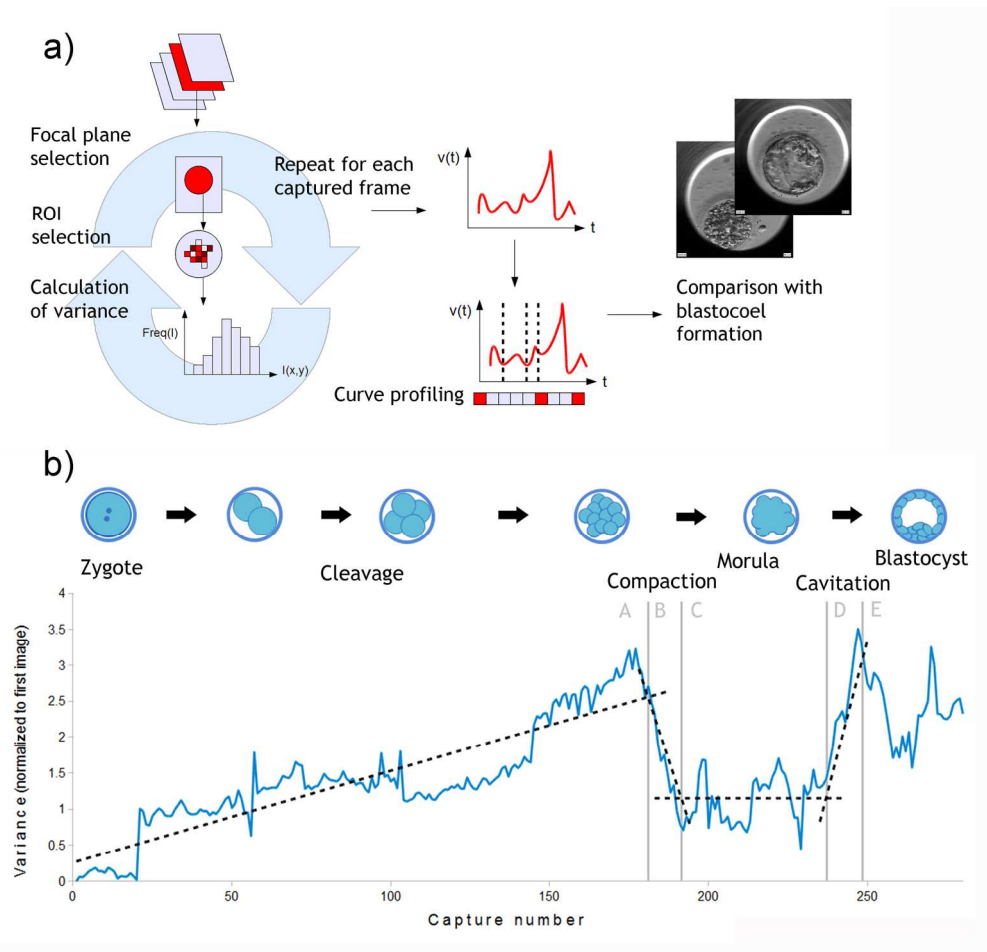


Figure 1: a) Illustration of computational pipeline of the captured image series of an embryo. The optimal focal plane from the image stack was selected. A region of interest (ROI) was selected within each individual image, and one value of the variance in image intensity was computed for each ROI. This process was repeated for each capture in the image series, resulting in a function $v(t)$ describing the variance as a function of time. $v(t)$ was then further analyzed for the occurrence of detectable key events, profiling the embryo development. Finally the profile for embryos forming blastocysts and not forming blastocysts were compared. b) Image intensity variance of an embryo during the course of 280 frame captures, normalized to the first image in the series. Divisions during the cleavage stage are detectable as sudden increases in image variance, due to the number of increased edges in the image, as blastomeres undergo mitosis. At the onset of compaction, individual blastomere membranes are no longer distinguishable, and the variance drops and remains at a low level during the morula stage. The variance increases once more as blastocoel expansion sets in, and may fluctuate strongly during the blastocyst stage, if the embryo displays several cycles of collapse and re-expansion. The growth of the embryo has been considered in five stages. A) Initial divisions from fertilization to onset of compaction. B) Onset to completion of compaction. C) Morula. D) Cavitation. E) Blastocyst. The mean and change in variance has been calculated for each section. Dashed trend lines have been added for illustrative purpose.

171x162mm (300 x 300 DPI)

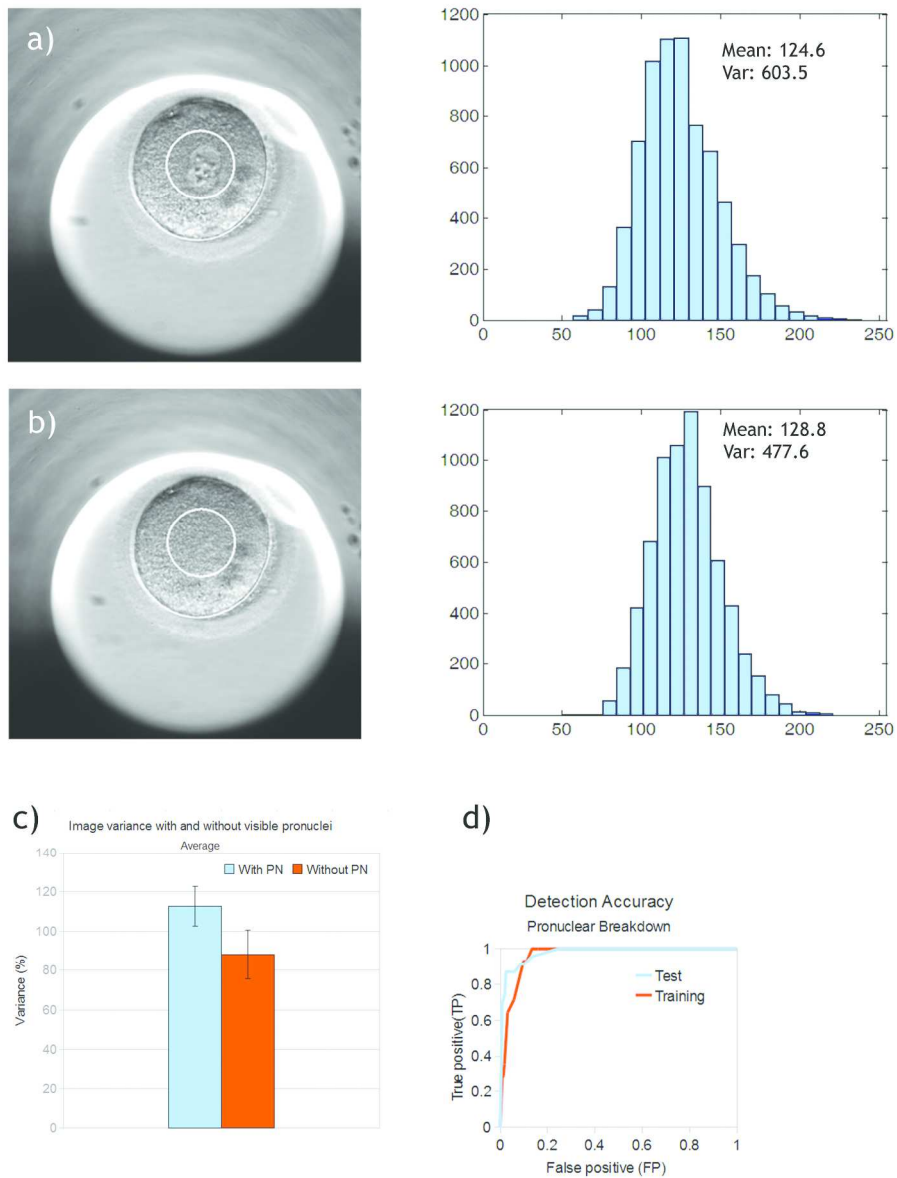


Figure 2: Calculation of variance in image intensity using pronuclei as an example. Images a) and b) were captured 20 min apart. The frequency of image gray scale values (0-255) within a selected ROI (white circle) at half embryo radius has been plotted as histograms, and the mean and variance calculated. c) Difference in image variance before (blue) and after (red) pronuclear breakdown. Standard deviation calculated as mean over the training set of 14 embryos ($p < 0.0001$). d) Detection accuracy of the training (14 embryos) and test (25 embryos) sets, respectively. The computation is governed by a single threshold (gradient of decreasing variance over time). Pronuclear breakdown is defined as gradients larger than some threshold, yielding an increase in true positive (TP) accuracy as the threshold decreases.
254x312mm (300 x 300 DPI)

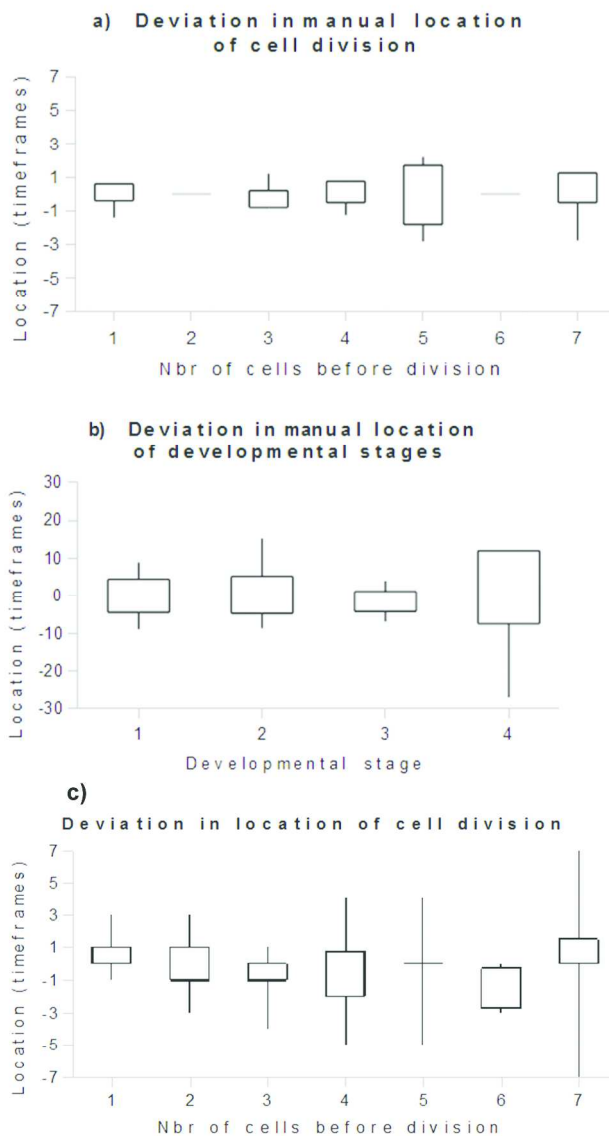
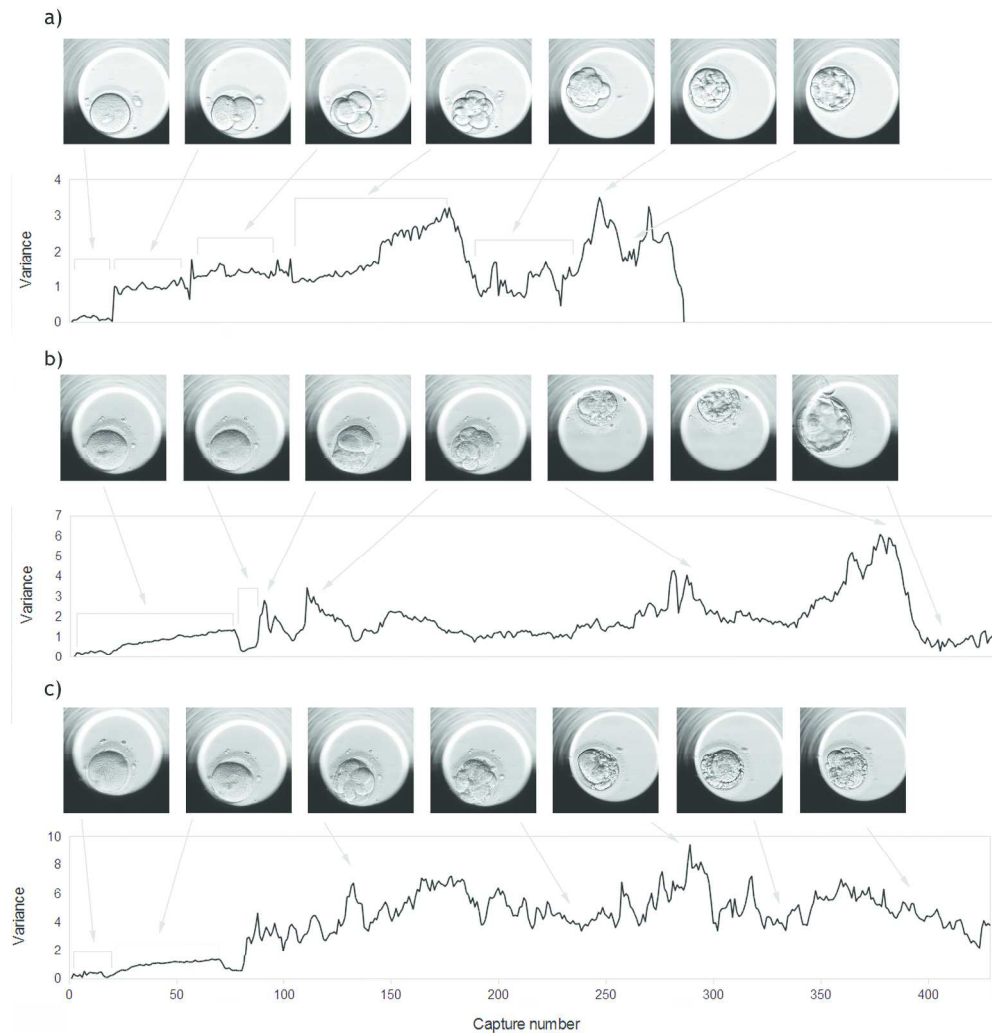


Figure 3: Standard deviation in manual annotation for the evaluation embryo in terms of a) timings of mitotic divisions up to 8 cells and b) detection of the beginning of developmental stages: 1-Compaction, 2-Morula, 3-Cavitation and 4-Blastocyst. Bars represent lower to upper quartile, whiskers minimum and maximum values. c) The deviation from expert determined location of division in terms of timeframes for the divisions that were detected, plotted vs the number of cells preceding the division. Bars represent lower to upper quartile, whiskers minimum and maximum values.

331x572mm (300 x 300 DPI)



43
44
45
46
47
48
49

Figure 4: Profile of three representative embryos showing decreasing quality (a-c). Variance was calculated from the image intensity at a circular region encompassing the center of the embryo. A few example images are shown at points where characteristic changes are visible in the variance profile. For a good quality embryo (a), mitotic divisions are visible as successive increases in image variance, and the morula stage as a period of lowered variance. b) illustrates a clearly expressed pronuclear breakdown, but experiences fragmentation during the cleavage stage, even though a blastocyst is eventually formed. In c), the pronuclear breakdown is also apparent, but the embryo develops early fragments, never reaching a blastocyst stage.

50
51
52
53
54
55
56
57
58
59
60

254x274mm (300 x 300 DPI)

1
2
3
4
5
6
7
8
9
10
11
12
13
14
15
16
17
18
19
20
21
22
23
24
25
26
27
28
29
30
31
32
33
34
35
36
37
38
39
40
41
42
43
44
45
46
47
48
49
50
51
52
53
54
55
56
57
58
59
60

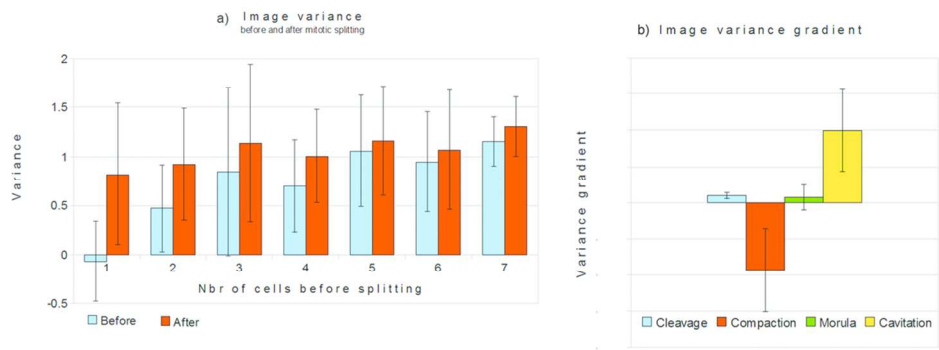


Figure 5: a) Average variance for 14 training embryos before and after mitotic splitting. P-values are $P < 0.05$ for first and second splitting, $P > 0.1$ for splitting 3-7. The negative variance before the first splitting is due to the drop in variance during syngamy. b) Gradient of image variance for embryo developmental stages for the 14 training embryos. $P < 0.001$ for adjacent stages.
108x39mm (300 x 300 DPI)

Peer Review

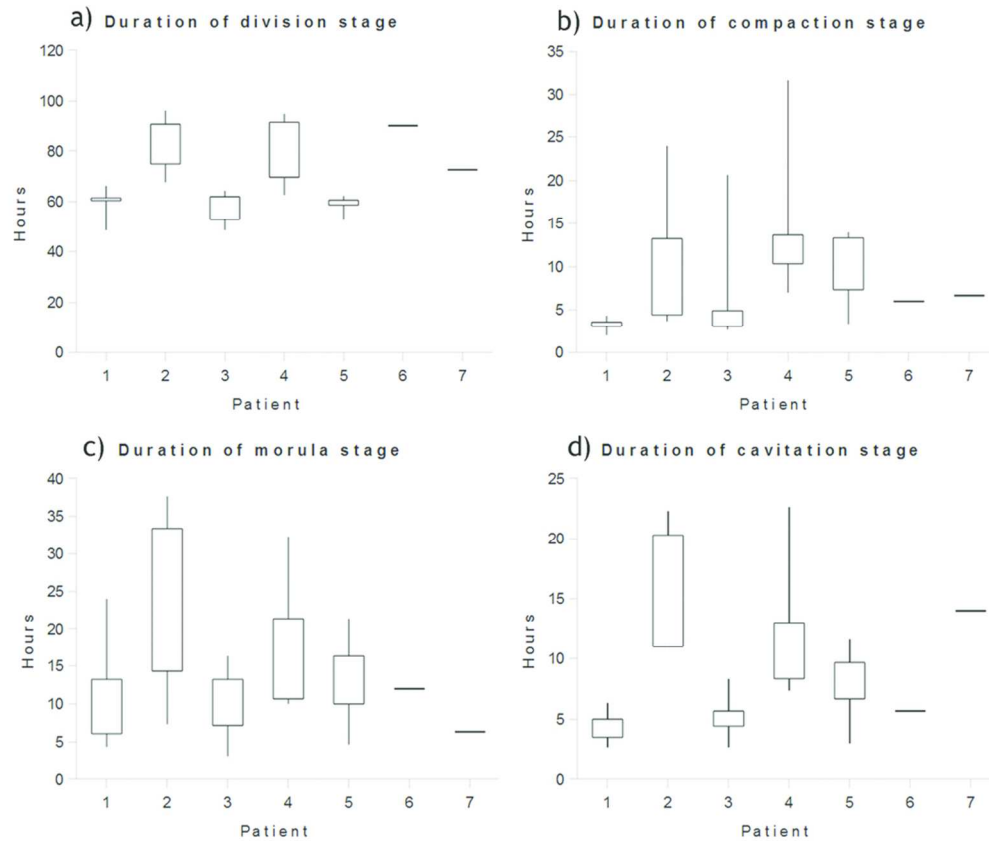


Figure 6: Duration in hours, automatically measured, of four stages of embryo development for seven patients (Total 28 embryos). a) Cleavage (the time from first frame to onset of compaction). b) Compaction (time from onset until completed). c) Duration of morula stage. d) Duration of cavitation stage (time from onset of cavitation to blastocyst). Patients 6 and 7 had only one embryo each completing all four stages. Bars represent lower to upper quartile, whiskers minimum and maximum values.
89x76mm (300 x 300 DPI)

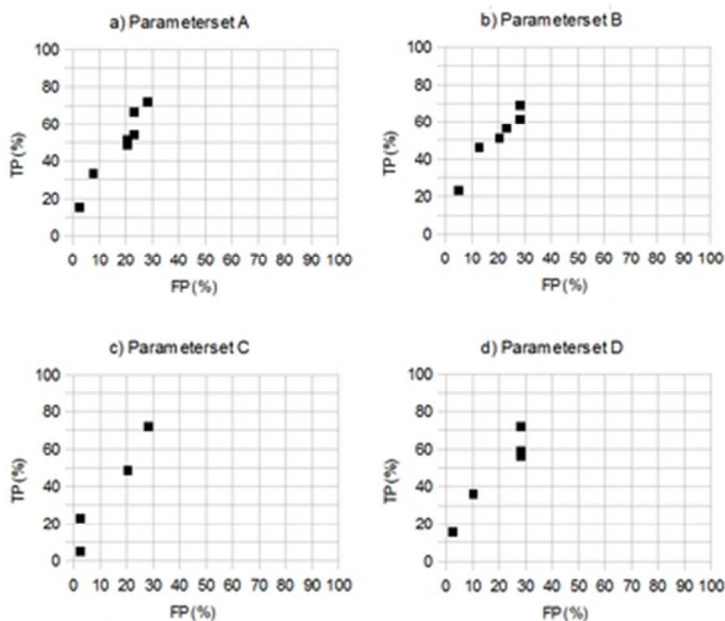


Figure 7: Example of the results in blastocoel detection using four different parameter sets. The parameters were:

A: $q_1 = 20$, $q_2 = 50$, $q_3 = 0.65$, $q_4 = 5$,

B: $q_1 = 20$, $q_2 = 10$, $q_3 = 0.65$, $q_4 = 5$,

C: $q_1 = 20$, $q_2 = 50$, $q_3 = 0.65$, $q_4 = 1$,

D: $q_1 = 20$, $q_2 = 50$, $q_3 = 0.65$, $q_4 = 10$,

where q_1 is relative location of first main gradient, q_2 is width of main gradient, q_3 is height of the main maxima and q_4 is maximum number of gradients. Weights were $w_1 = 0.15$, $w_2 = 0.15$, $w_3 = 0.3$, $w_4 = 0.4$ for all cases.

33x28mm (300 x 300 DPI)

Appendix

Nomenclature

1		
2		
3		
4		
5		
6		
7		
8		
9		
10		
11		
12	I	= image amplitude (grey scale)
13		
14	x, y	= Cartesian coordinates in image plane
15		
16	z	= Cartesian coordinate in direction of focus
17		
18	t	= time
19		
20	v	= image grey scale variance
21		
22	k	= time index
23		
24	n, m	= image dimension
25		
26	H	= H-maxima transform
27		
28	\bar{w}	= weights for linear combination of features
29		
30	R	= dimension of \bar{w}
31		
32	\bar{f}	= feature descriptor or image variance profile
33		
34	S	= dimension of \bar{w}
35		
36	M	= $I \cdot J$ dimensional mapping of features
37		
38	q	= parameters of M .
39		
40	r, s	= index of M .
41		
42		
43		
44		
45		
46		
47		
48		
49		
50		
51		
52		
53		
54		
55		
56		
57		
58		
59		
60		

Let the image intensity captured at focus z and time t be described as an intensity function $I(x,y,z,t)$, having the variance (for one $z = 0$),

$$v(t) = \frac{1}{n \cdot m} \cdot \sum_{x=1}^n \sum_{y=1}^m \left(I(x, y, t) - \overline{I(x, y, t)} \right)^2. \quad (\text{eq 1})$$

The gradient of variance is approximated as

$$\frac{dv(t)}{dt} \cong \frac{v(t_k) - v(t_{k-1})}{v(t_k)} \quad (\text{eq 2})$$

Appendix A: Focal selection

There are several algorithms for auto focusing of a microscope (1, 2, 3) where a calculation of a chosen focus function while iterating the focus in small steps, dz , is performed. In our case we had a set of already-captured images at fixed focal distance of the order of microns. It can be deduced from Fourier optics (4), that searching for focus is equivalent to searching for increased detail in images, *i.e.* high frequency changes in image intensity. Local maxima in image variance, $dv(z,t)/dz$, will correspond to high frequency changes in the image, but since we do not necessarily know the way in which the physical focus has been moved, the second derivative is computed and solved for:

$$\frac{d^2v(t)}{dt^2} = 0. \quad (\text{eq 3})$$

Results show that HMC embryo images exhibits a higher variance at one end of the focal stack. This is due to the image artefacts from the optics, causing visible accentuated edges, alternating in darker and brighter bands around the blastomeres (Figure A1g). When the focus moves further up the well (Figure A1a), the same effect is observed on the edges of the well. To avoid contributions from the well, the image centre was cropped out prior to calculation. For each stack, the image closest to fulfilling the condition (eq 3) was chosen as the optimally focused (Figure A1h).

Appendix B: Detection of location of pronuclei breakdown

The pronuclei breakdown is defined as

$$\frac{dv(t)}{dt} \leq v_{lim} < 0. \quad (\text{eq 4})$$

Appendix C: Detection of location of mitotic divisions

A mitotic splitting is defined as

$$\frac{dv(t)}{dt} \geq v_{lim} > 0. \quad (\text{eq 5})$$

A Figure C1 shows an example.

Appendix D: Detection of blastocyst formation

The variance (eq 1) was computed for the selected region of interest for each image in the time series at the selected focal plane, reducing the initial $I(x,y,z,t)$ to $v(t)$. Several features, such as number of local maxima, local maxima height and gradient steepness as a function of t were extracted from the shape of the function $v(t)$.

Local maxima were detected in the following manner:

$$v_{lm} = v_s(t) - H(v_s(t)) > v_{lim}, \quad (\text{eq 6})$$

where H is an H-maxima transform, $v_s(t)$ is $v(t)$, smoothed by a moving average filter spanning 20 time frames, and v_{lim} is a variance threshold, chosen using the image training set. Local variance gradients were detected in the following manner:

$$v_{lg} = \frac{dv_s(t)}{dt}, \quad (\text{eq 7})$$

where the gradient of $v(t)$ is computed according to (eq 2), and $v_s(t)$ is $v(t)$, smoothed by a moving average filter spanning 20 time frames. After detection, the following filtering was performed:

- 1) Local maxima or gradients with a width $t_{lim} < t_{max} - t_{min}$, were discarded, where $v_{lm}(t) > 0$ for all $t_{min} < t < t_{max}$.
- 2) All local maxima or gradients were counted as one region, if separated by a distance $t < t_{dist}$.

t_{lim} and t_{dist} were determined using the training image set to 10 time frames and 25 time frames, respectively, corresponding to 1h 20min and 4h 20 min at the current capture frequency.

The profile of position, height and width of local maxima and local gradients were combined in a feature vector \bar{f} , thus performing a dimension reduction of the original image time series, where \bar{f} here works as a feature descriptor. The feature vector \bar{f} can then be transformed into a probability $P \in [0,1]$:

$$P = \bar{w}^T \cdot M(q) \cdot \bar{f} \quad (\text{eq 8})$$

where $M(q)$ is a $R \cdot S$ matrix mapping, controlled by a set of parameters q , and \bar{w} is a vector of weights of dimension R . P is the scalar probability that the embryo displays the condition in question. Here, \bar{f} (of dimension S) can be thought of as a set of symptoms, and the combination $\bar{w} \cdot M(q)$ performs the mapping which transforms the symptoms into a probability that a specific state is present. For this study, the following components of \bar{f} were chosen:

f_1 = location of the first major local maxima, according to (eq 6).

f_2 = location of the first negative gradient, according to (eq 7).

f_3 = width of the main negative gradient, as calculated by (eq 7).

f_4 = the height of the main local maxima detected, as calculated by (eq 6).

f_5 = the mean height of the local maxima detected after f_4 , as calculated by (eq 6).

f_6 = the number of detected local maxima, as calculated by (eq 6).

The components of \bar{f} were then combined using the mapping M , having the following non-zero components:

$$M_{12} = \begin{cases} 1, (f_2 - f_1)/f_1 \geq q_1 \\ 0, (f_2 - f_1)/f_1 < q_1 \end{cases} \quad (\text{eq 9})$$

describing the relative position of maximum variance and negative gradient at compaction (stage AB and B), where q_1 is the minimum allowed separation.

$$M_{33} = \begin{cases} 1, f_3 \geq q_2 \\ 0, f_3 < q_2 \end{cases} \quad (\text{eq 10})$$

describing the width of the main negative gradient (duration of the compaction stage B), where q_2 is the minimum allowed width.

$$M_{45} = \begin{cases} 1, f_5 \geq q_3 \cdot f_4 \\ 0, f_5 < q_3 \cdot f_4 \end{cases} \quad (\text{eq 11})$$

describing the relationship between the major local maxima at cavitation (DE) and any following maxima, indicating blastocoel fluctuations. q_3 = maximum relative height.

$$M_{66} = \begin{cases} 0, f_6 \geq q_4 \\ 1, f_6 < q_4 \end{cases} \quad (\text{eq 12})$$

allowing for only a finite number of negative gradients to be found, as a heavy fragmented embryo tends to fluctuate more. q_4 = maximum allowed number.

For this choice of mapping, $R = 4$ and $S = 6$. A linear combination of the component was calculated using the weights \bar{w} :

$$P = \sum_{r=1}^R \sum_{s=1}^S (w_s M_{rs}(q)), \quad (\text{eq 13})$$

where $P \in [0,1]$ yields a measurement of the possibility of blastocyst formation. A minimum threshold P_{lim} can then be used to define all blastocysts as $P > P_{lim}$.

References

- 1
2
3
4
5
6
7 [1] Groen FCA, Young IT, Ligthart G. A comparison of different focus functions for use in autofocus
8 algorithms. *Cytometry* 1985;6:81-\$91.
9
10 [2] Geusebroek JM, Cornelissen F. Robust autofocusing in microscopy. *Cytometry* 2000;39:1-\$9.
11
12 [3] Sun Y, Duthaler A. Autofocusing in computer microscopy: selecting the optimal focus algorithm.
13 *Microsc Res Tech* 2004;65:139-\$149.
14
15 [4] Papoulis A. *The Fourier Integral and its Applications*. 1962.
16
17
18
19
20
21
22
23
24
25
26
27
28
29
30
31
32
33
34
35
36
37
38
39
40
41
42
43
44
45
46
47
48
49
50
51
52
53
54
55
56
57
58
59
60

For Peer Review

1
2
3
4
5
6
7
8
9
10
11
12
13
14
15
16
17
18
19
20
21
22
23
24
25
26
27
28
29
30
31
32
33
34
35
36
37
38
39
40
41
42
43
44
45
46
47
48
49
50
51
52
53
54
55
56
57
58
59
60

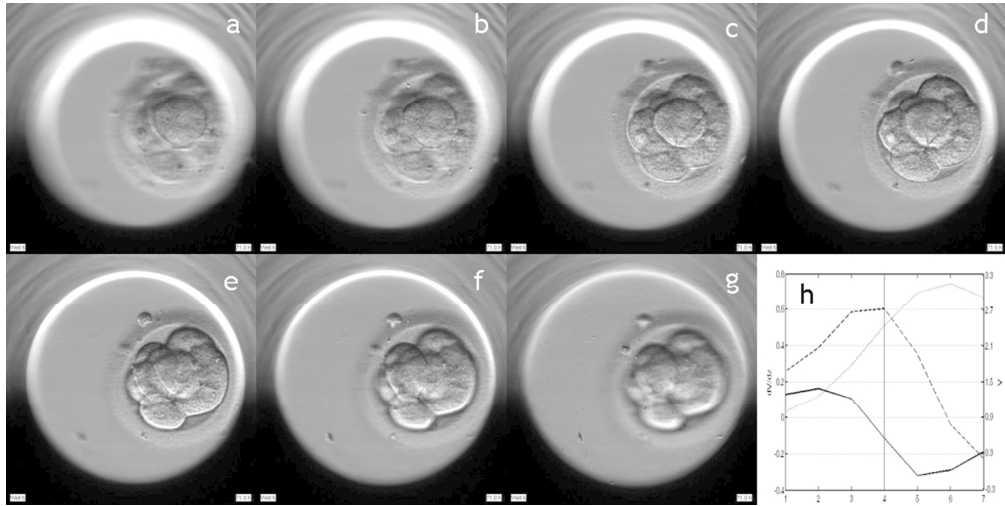


Figure A1: a-g) Embryo images captured at seven different focal planes. h) Variance of image intensities (dotted), gradient of variance (dashed) and second gradient of variance (solid) (arbitrary units). Vertical line marks the selected plane in optimal focus.
101x50mm (300 x 300 DPI)

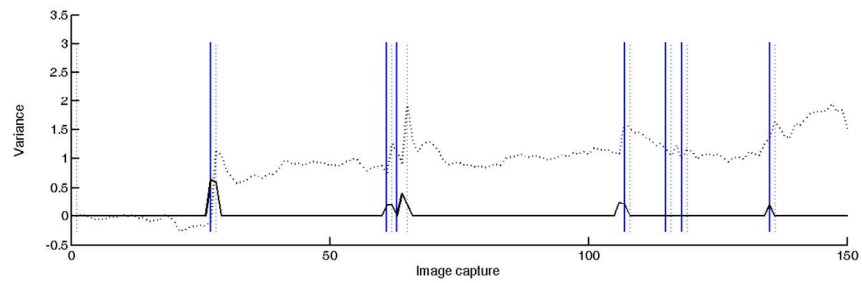


Figure C1: Example of detection of cell division Dashed black: variance of an embryo during 150 frames. Vertical lines: Manually detected cell divisions for comparison with division beginning on solid line, ending on dotted. Solid black: Peaks represents detected gradients. Two cell division around frame 120 only gave very weak signal and have not been detected.

361x115mm (96 x 96 DPI)